SKB

Task 10.2.2 – Modelling flow and flow channelling in a fracture under normal loading

Task 10 of SKB Task Force GWFTS – Validation approaches for groundwater flow and transport modelling with discrete features

Paolo Trinchero

Liangchao Zou

Aitor Iraola

SVENSK KÄRNBRÄNSLEHANTERING

Task 10.2.2 – Modelling flow and flow channelling in a fracture under normal loading

Task 10 of SKB Task Force GWFTS – Validation approaches for groundwater flow and transport modelling with discrete features

Paolo Trinchero[1], Liangchao Zou[2], Aitor Iraola[1]

1 Amphos 21 Consulting S.L.
2 KTH Royal Institute of Technology

Abstract

This report summarises the work performed by Amphos 21 and KTH, as a joint modelling group, in the framework of the modelling activities of the SKB Task Force on Groundwater Flow and Transport of Solutes (GWFTS). Task 10.2.2 focuses on a hydromechanically (HM) coupled flow test performed on a rock sample that includes a single natural fracture. The modelling work is carried out using an uncoupled approach: first, changes in fracture aperture as a function of normal load are computed using an elastic-plastic contact model, and second, water flow at the different loading stages is simulated using Reynolds equation. The three metrics required by the prediction-outcome exercise (aperture distributions, flowrates and channelling factors at the different loading stages) are reported in separate tables. Besides, additional results, such as plots of the groundwater velocity fields and additional interpretations of the evolution of flowrates, are discussed. Moreover, comparison with the experimental data (provided to the modelling team *a posteriori*) are also presented. The comparison between experimental and modelling results highlights the significant overestimation of flowrates of models based on the local cubic law.

Sammanfattning

Denna rapport sammanfattar det arbete som utförts av Amphos 21 och KTH, som utgjort en gemensam modelleringsgrupp, inom ramen för modelleringsaktiviteterna i SKB Task Force on Groundwater Flow and Transport of Solutes (GWFTS). Modelleringsuppgift 10.2.2 fokuserar på ett hydromekaniskt (HM) kopplat flödesexperiment som utförts på ett bergprov som inkluderar en enda naturlig spricka. Modelleringsarbetet har utförts med ett okopplat angreppssätt: först är förändringar i spricköppningen som funktion av belastning i normalriktningen beräknad med hjälp av en elastisk-plastisk kontaktmodell och sedan är vattenflödet vid de olika belastningsfallen simulerad med Reynolds ekvation. De tre mät-värdena som efterfrågas i denna prediktion-resultatövningen (aperturfördelningar, flödeshastigheter och kanalfaktorer vid de olika belastningsfallen) rapporteras i separata tabeller. Dessutom diskuteras ytterligare resultat, såsom grafer av grundvattenhastighetsfält och ytterligare tolkningar av utvecklingen av flödeshastigheter. Dessutom presenteras jämförelser med experimentella data (tillhandahölls till modelleringsteamet *a posteriori*). Jämförelsen mellan modelleringsresultat och experimentella dito belyser den betydande överskattningen av flödeshastigheter som görs av modeller baserade på en lokal kubisk lag.

Contents

1   Introduction

The work summarised in this report is carried out within the framework of Task 10.2, whose general objectives are (Bruines, unpublished)[1]:

- The development of concepts and models for flow and transport at the single fracture scale.

- The consideration of the importance of hydro-mechanical coupling (normal loading only) on flow and transport.

- The development of modelling approaches for prediction of (i) flow and transport in single fractures and (ii) upscaled fracture properties from borehole to deposition hole scale.

- To build a starting point for pragmatic validation, i.e. a prediction-outcome exercise, as described in the White Paper.

More specifically, this work is part of Task 10.2.2, in which flow through a single fracture under different normal loads is investigated and modelled.

The work is carried out using an uncoupled approach: a contact model (Zou et al., 2020) is first used to compute apertures at different normal loads. The different computed apertures are the basis for the flow calculations, which are carried out using a depth-averaged approach based on laminar flow assumption and the local cubic law. Sensitivity analyses are performed by adding a correction factor to the local cubic law. Moreover, alternative calculations are performed, based on explicit consideration of the 3D fracture aperture and the Navier-Stokes equations.

All the results presented here are based on a blind prediction exercise, i.e. the modelling team was not aware of the actual flowrates obtained during the HM experiment. A comparison of the results presented here with the experimental results constitutes the basis for both model validation and for future model calibrations.

---

[1] Bruines P. SKB Task Force on Modelling of Groundwater Flow and Transport of Solutes: Description of Task 10.2. SKB R-23-10, Svensk Kärnbränslehantering AB, Stockholm, Sweden. Unpublished.

2 Description and objectives of Task 10.2.2

Task 10.2.2 focuses on a hydromechanically (HM) coupled flow tests performed at the Borås facilities of Research Institutes of Sweden (RISE) on a $20 \times 20 \times 25$ cm^3 rock sample that includes a single "simple" natural fracture (Jacobsson and Godio, 2023; Godio and Jacobsson, 2024). The rock sample, which was obtained from the Flivik rock quarry in Sweden, contains a quasi-parallel natural fracture (Figure 2-1).

2.1 Objectives of Task 10.2.2

The specific objectives of this task are:

1) Prediction and validation of the upscaled fracture geometry from borehole sized fracture geometry and/or fracture trace geometry.

2) Prediction and validation of flow across a fracture subject to different normal stresses.

3) Support the development and demonstration of pragmatic validation workflow at the single fracture scale.

Amphos 21 did not participate in Task 10.2.1 and thus only general objectives 2) and 3) above are also objectives of the Amphos modelling team.

The work summarised in this report is very much in line with the general objectives of Task 10.2, which is to understand flow and transport processes through natural fractures under normal loading conditions.

Figure 2-1. *Block 19.6.1.4 from which the sample is cut (left) and Slab of 19.6.1.4 block from which the $200 \times 200 \times 250$ mm^3 is cut (right). Figure taken from Bruines (unpublished)[2].*

---

[2] Bruines P. SKB Task Force on Modelling of Groundwater Flow and Transport of Solutes: Description of Task 10.2. SKB R-23-10, Svensk Kärnbränslehantering AB, Stockholm, Sweden. Unpublished.

2.2　Limitation of Task 10.2.2

The main limitation of the experimental work, and thus of the related numerical interpretation, is related to the very specific nature of the fracture under consideration, which is extracted at a relatively shallow depth and does show only limited mineral precipitation. Natural fractures found at repository depth were subject to completely different rock stress history, temperature and geochemical hydrothermal events. Thus, caution should be used when extrapolating the results of Task 10.2.2 to real applications relevant for safety assessment studies.

In the conclusion section it is also discussed how some of the presented results, namely the correction factor applied to the local cubic law, could be made more generic by applying the same methodology on a broader range of "fracture types".

2.3　Data description

The experimental data used in Task 10.2.2 have been obtained as part of an extension of the POST project. The main objective of the POST (Parameterisation of structures) project is to develop a strategy and guidelines for determining the parameters necessary for assessing fracture stability at the repository scale for repository design and post-closure analysis used for the KBS-3 disposal concept.

The data that the POST 2 project shared with the Task Force are:

1. geometrical data of the unopened and opened rock sample.

2. contact pressure measurements using pressure sensitive film.

3. results of the hydromechanically coupled flow tests carried out on the rock sample.

4. intact rock properties from previous tests on the rock from the same location.

Geometrical data (point 1), specifically high-resolution scanning of the two fracture surfaces, have been used to set initial conditions (initial fracture aperture) for the contact analysis. Namely, the following two files have been used:

• Complete_lower_part_after_first_opening.csv

• Complete_upper_part_after_first_opening.csv

Intact rock properties (point 4) have been used to parameterise the contact model whereas the LVDT measurements (point 3) have been used to calibrate the initial aperture while other data, primarily flowrates, will be used for model validations. Both LVDT displacement data and flowrates are included in the Excel file "Flow_tests_bcs_with_displacements_and_flows.xlsx".

It is explicitly recognised that the information contained in the above files carries an associated uncertainty (both in terms of initial fracture aperture and measured displacements). The treatment of this uncertainty is discussed throughout the paper (e.g. Section 3.1.5).

Contact pressure measurements (point 2) have been analysed, but a thorough interpretation has been found difficult due to the loss of material during the fracture opening. Therefore, contact pressure measurements are not included in this report.

The different phases of the HM test are described in detail in the Task Description (TD) document (Section 4.3.1).

2.4　Pragmatic validation

The pragmatic validation is done following the guidelines provided in Section 4.5 of the TD. In particular, the exercise is carried out as a prediction/outcome exercise and the following deliverables are produced:

1. Aperture distributions at normal stresses 0, 1 and 4 MPa.

2. Flow rates at normal stresses 0, 1 and 4 MPa.

Validation of point 1 above is done by comparing modelling results with the average displacements computed by the LVDTs. Given the high uncertainty of the initial aperture estimated from the fracture scan data (e.g. material loss, difficulty in placing the two scanned fracture surfaces in the same reference system, etc), a preliminary step was required which consisted of defining an equivalent initial aperture by moving the two fracture surfaces together and comparing the results obtained using a Navier-Stokes based computational fluid dynamics (CFD) model with the experimental flowrate obtained for unloaded conditions. See Trinchero et al. (2024) for further discussion on this point. This step precedes model validation and is necessary to obtain a reliable starting point for model validation. The derivation of this initial fracture aperture is referred to as "calibration" in the reminder of this document.

Point 2 above is validated by comparing the computed flowrates with the experimental results. Notice that in this report all the numerical results have been computed in "blind-prediction mode" and the comparison with experimental results is done *a posteriori*. Future work will entail further model calibration to improve the match with experimental results.

Besides the prediction/outcome exercise, other items were proposed (see Bruines, unpublished)[3] and are discussed next:

- *Model purpose.* This is very briefly discussed in Section 3.1.1.

- *Model applicability*. The model is, in principle, intended to be applied to the considered fracture only. A quantitative argument for generalising this model to a wider range of fractures could be made by relating the results of this study (e.g. ratio of hydraulic to mechanical aperture) to underlying roughness characteristics, which could be quantified using standard metrics such as JRC (Barton and Choubey, 1977). However, this extrapolation is beyond the scope of this report.

- *Determination of critical aspects*. This is discussed in Section 3.1.3.

- *Performance measures and criteria*. This point has not been assessed here, but it basically implies to define some acceptance criteria related to the measured flowrate (e.g. predicted flowrate within the some established limit of the measured value).

- *Conceptual assumption* and *approaches for derivation of numerical parameters being tested by the Pragmatic Validation exercise*. This is discussed in Section 3.1.2.

- *Understanding of the scope and limitations of experimental data and theoretical concepts being used to support modelling and performance measures*. This point has been only partly addressed in this work. The limitations of the theoretical aspects and approaches used is thoroughly discussed in this report. However, data has been taken as such, without any systematic assessment of the related experimental limitations. Additional results, not presented here but summarised in an accompanying paper (Trinchero et al. 2024), have more carefully considered the uncertainty related to fracture aperture data.

- *Pragmatic validation statement*. The prediction/outcome exercise has pointed out a relatively low level of confidence in the model predictions However, further analysis of the models, based on the modified Local Cubic Law (LCL,) has pointed out that the typical employed modelling approaches based on LCLcan still be applied to predict flow across natural fractures subject to variable normal loads, provided that a robust relationship between mechanical and hydraulic aperture is established.

---

[3] Bruines P. SKB Task Force on Modelling of Groundwater Flow and Transport of Solutes: Description of Task 10.2. SKB R-23-10, Svensk Kärnbränslehantering AB, Stockholm, Sweden. Unpublished.

3 Modelling and methodology

3.1 Modelling Task 10.2.2

3.1.1 Model purpose

As stated in Section 4.4 of the TD (Bruines, unpublished)[4], "the main purpose of Task 10.2.2 is to better understand the effect of normal stresses perpendicular to a natural fracture on the flow and transport through such a fracture". However, the focus and scope of the work performed by Amphos 21 (A21) and KTH, the Royal Institute of Technology in Stockholm, and summarised here is limited to flow, i.e. we are assessing here the possibility to reliably predict flow along a natural fracture subject to normal load.

3.1.2 Model description

The methodology used for the modelling of Task 10.2.2 is summarised in Figure 3-1 and is as follows:

1. The initial fracture scan data (*Complete_lower_part_after_first_opening.csv* and *Complete_upper_part_after_first_opening.csv*) has been used to compute the initial fracture aperture, which is defined as the difference between the height of the upper surface and the height of the lower surface. This initial aperture has been calibrated using a CFD model (see discussion in Section 2.4).

2. The contact analysis is carried out using a contact model based on a boundary element model (Tian and Bhushan, 1996; Zou et al., 2020).

3. The different aperture fields, compute at different normal loads, have been used to set-up continuum models, where the local cubic law (Witherspoon et al., 1980) has been used to map aperture to equivalent permeability. Groundwater flow simulations have been carried out using the finite difference numerical code MODFLOW-2005 (Harbaugh et al., 2000).

4. Particle tracking simulations have been run using the numerical code RW3D (Fernandez-Garcia et al., 2005).

There are a number of assumptions that should be mentioned:

- About step 1 above, it is worthwhile mentioning that the initial aperture has been calibrated to fit the average LVDT displacement. This fit was achieved by reducing the whole initial aperture, as provided by the scan data, by a value of 1.2×10^{-4} m. When performing this shift, those values where aperture becomes negative, are considered as contact points.

- About step 3 above, laminar flow and depth averaged properties (i.e. 2D flow model) are assumed. In a parallel modelling work, aperture has been fully resolved and the Navier-Stokes equation has been solved (see Appendix).

It is worth spending a few words on how the initial aperture was estimated from the scan data. The surface roughness data obtained from scanning the two fracture surfaces provides detailed information about the topography of the two surfaces, i.e. the height variations across the fracture surface, representing the peaks and valleys. To derive the initial aperture, it is first necessary to allign the two fracture surfaces based on the same reference system. This step was done by RISE and is acknowledged to be error prone. Secondly, the roughness data of the two surfaces are interpolated in a regular grid and thirdly the aperture at each point of the regular grid was calculated as the difference between the height of the upper and lower surfaces.

---

[4] Bruines P. SKB Task Force on Modelling of Groundwater Flow and Transport of Solutes: Description of Task 10.2. SKB R-23-10, Svensk Kärnbränslehantering AB, Stockholm, Sweden. Unpublished.
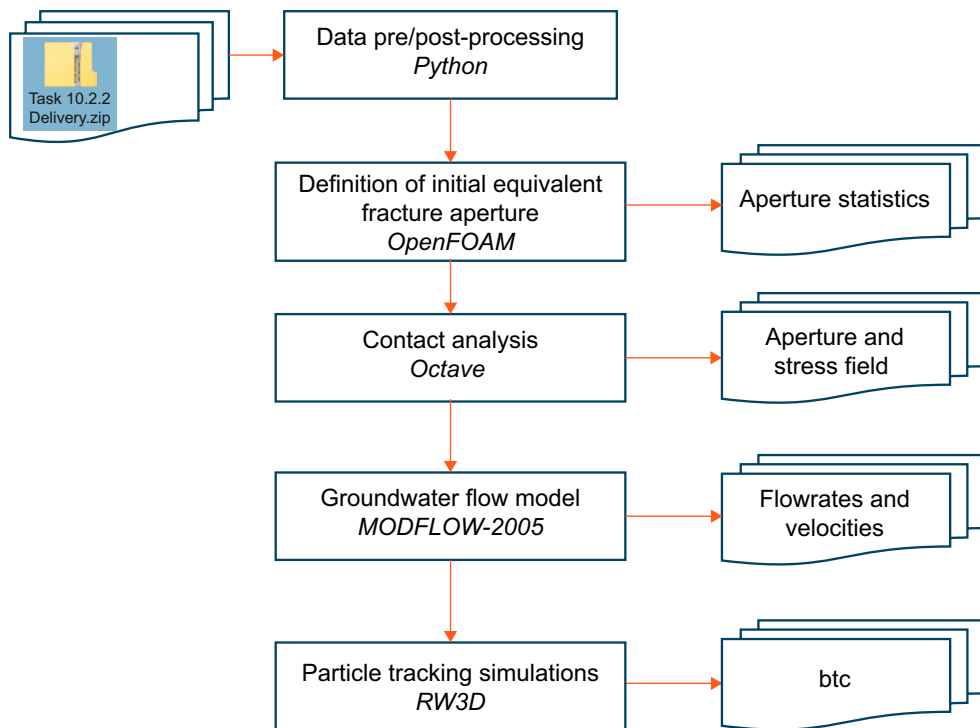
Figure 3-1. *Modelling flowchart of Task 10.2.2.*
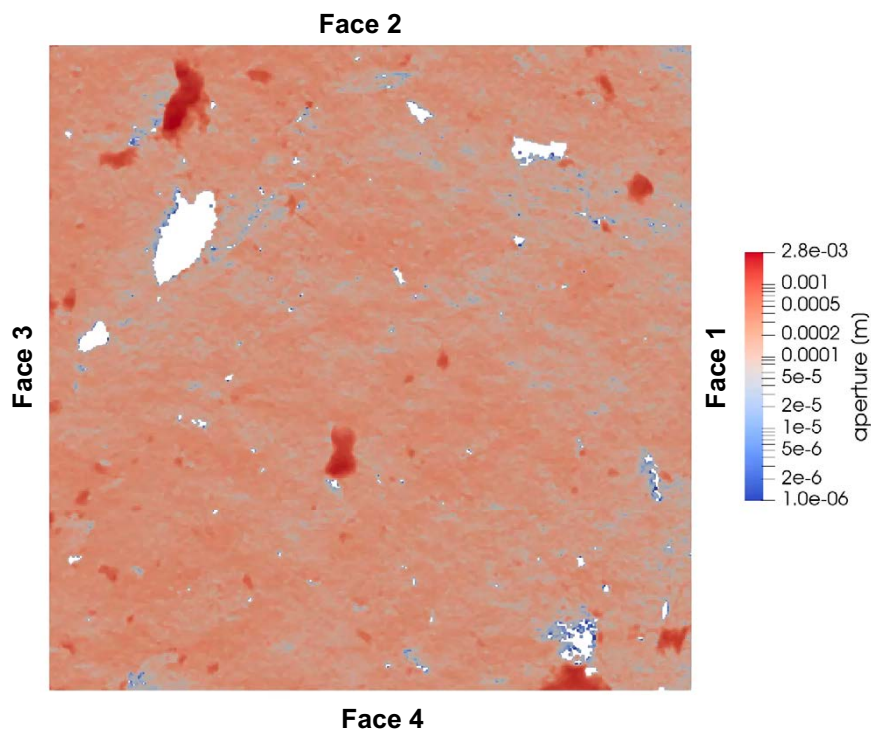
Figure 3-2. *Conventions used to define the two different flow directions. The plot shows the aperture distribution for unloaded conditions (initial state). White areas are contact points.*

The key equations of the elastic-plastic contact model used in this report are briefly summarized below. More detailed theory can be found in Tian and Bhushan (1996) and Zou et al. (2020).

For a contact system with two rough elastic surfaces, the total complementary potential energy, V^*, is given by (Tian and Bhushan 1996)

$$V^* = \frac{1}{2} \iint_\Omega \sigma_n \bar{u}_z(x,y) dxdy - \iint_\Omega \sigma_n \bar{u}_z^*(x,y) dxdy \qquad\qquad \text{Equation 3-1}$$

where Ω is the surface domain, σ_n is the local normal stress, $\bar{u}_z(x,y)$ is the composite surface normal displacement in Ω, and $\bar{u}_z^*(x,y)$ is the total displacement of the two contacting asperities inside the assumed contact area based on geometrical interference, which can be determined using the following contact conditions:

$$\bar{u}_z^*(x,y) + e(x,y) - \delta = 0, \sigma_n > 0 \text{ for each point within contact area } C \qquad\qquad \text{Equation 3-2}$$

$$\bar{u}_z^*(x,y) + e(x,y) - \delta > 0, \sigma_n = 0 \text{ for each point outside contact area } C \qquad\qquad \text{Equation 3-3}$$

where $e(x,y) = |z_1(x,y) - z_2(x,y)|$ is the initial separation of the two surfaces and δ is the rigid-body movement under the applied normal stress.

The relationship between the normal displacement and the normal stress is given by the Boussinesq solution for normal distributed load on the surface of a semi-infinite body, expressed as:

$$\bar{u}_z(x,y) = \iint_\Omega A_{zz}(x,y,\xi,\eta) \, \sigma_n(\xi,\eta) d\xi d\eta \qquad\qquad \text{Equation 3-4}$$

where $A_{zz}(x,y,\xi,\eta)$ is the influence function for normal deformation at the surface location (x,y) due to a unit stress at surface position (ξ,η). This influence function can be calculated by:

$$A_{zz}(x,y,\xi,\eta) = \frac{1}{\pi E^* \sqrt{(x-\xi)^2 + (y-\eta)^2}} \qquad\qquad \text{Equation 3-5}$$

where E^* is the effective Young's modulus of the two surface materials, defined by the reciprocal of

$$\frac{1}{E^*} = \frac{1-v_1^2}{E_1} + \frac{1-v_2^2}{E_2} = \frac{2(1-v^2)}{E} \qquad\qquad \text{Equation 3-6}$$

where $E_1 = E_2 = E$ are the Young's moduli and $v_1 = v_2 = v$ are the Poisson ratios of the rock matrix that are assumed to be equal for the upper and lower blocks.

It is assumed that the rock asperity deforms as an elastic-perfectly plastic material and plastic deformation is confined within a local, small area, i.e. the elastic contact model is extended for elastic-plastic contact analysis. More specifically, in the contact of two rough surfaces, the normal stress is concentrated on the contact points and the perfectly plastic behaviour occurs on the contacting points (the intact rock is at the elastic state). Once the local stress at a contact point overcomes the yield limit (indentation hardness), the local asperity breaks (undergoes permanent deformation without any increase in stress). When considering perfectly plastic deformation, the dissipation of energy caused by plastic deformation needs to be added to the total complementary potential energy, written as (Tian and Bhushan, 1996):

$$\Delta V^* = \frac{1}{2} \iint_\Omega \sigma_n \bar{u}_z(x,y) dxdy - \iint_\Omega \sigma_n [\bar{u}_z^*(x,y) - \frac{1}{2}\Delta u_z^p(x,y)] dxdy \qquad\qquad \text{Equation 3-7}$$

where $\Delta \bar{u}_z^p(x,y)$ is the composite incremental surface displacement in the plastic deformation zone where the local contact stress reaches the (indentation) hardness of the rock matrix, H, i.e., $\sigma_n(x,y) > H$. It means that the (indentation) hardness is used as the yield stress limit for perfectly plastic deformation. Therefore, the yield condition is that the local normal stress should not exceed the yield stress, i.e., $\sigma_n(x,y) \leq H$. An equivalent total displacement of the two-contacting asperity for the elastic-plastic deformation regime can be defined as $\bar{u}_z^*(x,y) - \frac{1}{2}\Delta u_z^p(x,y)$, and $\Delta u_z^p(x,y)$ is given by Tian and Bhushan, (1996):

$$\Delta u_z^p(x,y) = \Delta \bar{u}_z^p(x,y)[1 + \frac{E_1(1-v_1{}^2)}{E_2(1-v_2{}^2)}]^{-1} = \frac{1}{2}\Delta \bar{u}_z^p(x,y) \qquad \text{Equation 3-8}$$

where $\Delta \bar{u}_z^p(x,y)$ is the incremental displacement of two contact surfaces where the stress reaches the rock hardness.

To solve the governing equation (Equation 3-7), the surface domain is discretized by a structured mesh, which is consistent with the digital topography of the rough surfaces (see details in Section 3.1.4). After discretization, Equation 3-7 can be expressed as

$$\Delta V^* = \frac{1}{2}\boldsymbol{\sigma}^T \cdot \boldsymbol{K} \cdot \boldsymbol{\sigma} - \boldsymbol{\sigma}^T \cdot \boldsymbol{u} \qquad \text{Equation 3-9}$$

where $\boldsymbol{\sigma}^T$ is the vector of stress, $\boldsymbol{K}$ is the influence matrix and $\boldsymbol{u}$ is the vector of normal displacement. The V^* has a minimum value with $\boldsymbol{\sigma}$ when

$$\nabla V^*(\boldsymbol{\sigma}) = \boldsymbol{K} \cdot \boldsymbol{\sigma} - \boldsymbol{u} = 0 \qquad \text{Equation 3-10}$$

Therefore, we obtain a linear complementarity problem, which aims to find the stress, $\boldsymbol{\sigma}$, and the contact area, C, satisfying:

$$\nabla V^*(\boldsymbol{\sigma}) = \boldsymbol{K} \cdot \boldsymbol{\sigma} - \boldsymbol{u} = 0$$

$$\text{s.t.}\ \boldsymbol{\sigma} > 0, \text{ for elements } I \in C \text{ and } \sum \boldsymbol{\sigma} A = F \qquad \text{Equation 3-11}$$

where A is the area of an element. A constrained conjugate gradient algorithm (Polonsky and Keer, 1999) is used to iteratively solve the contact pressure with an assumed incrementally increased normal stress, until it satisfies the convergence conditions that $\boldsymbol{\sigma} > 0$ and the summation of σA equals the applied total load F.

For the elastic-plastic analysis, an additional iteration is needed for each incremental step to determine the plastic deformation regime and magnitude based on Equation 3-8. Currently, the rock hardness is typically measured from rock samples with smooth surfaces, the hardness of rock matrix with surface roughness remains an open question and thus an uncertain parameter (see Section 3.1.4 for details on how this uncertainty has been treated). For contact analyses, the hardness values of rough rock matrix are often determined by calibration with compression experiment data (Kling et al., 2018; Zou et al., 2020; Li et al., 2021). Nevertheless, the ranges of this parameter have been discussed or determined through calibration in previous studies (e.g., Kling et al., 2018; Zou et al., 2020; Li et al., 2021). In addition, we demonstrated the sensitivity of hardness by using two cases with different hardness values.

In the main calculations, local fracture aperture, as computed by the contact model, was converted into local transmissivity using the local cubic law (LCL) (Witherspoon et al., 1980):

$$T(\mathbf{x}) = \frac{\delta(\mathbf{x})^3 \rho g}{12\mu} \qquad \text{Equation 3-12}$$

where ρ is the water density, μ is the water dynamic viscosity and g is the gravitational acceleration.

Sensitivity analyses were also performed by adding a correction factor, $f(-)$, to Equation 3-12:

$$T(\mathbf{x}) = \frac{[f \cdot \delta(\mathbf{x})]^3 \rho g}{12\mu} \qquad \text{Equation 3-13}$$

The main model limitations are:

- The modelling flowchart presumes a one-way coupling between mechanical and flow processes. Particularly for unloaded conditions, the high fluid pressure used at the fracture inlet might have some impact on fracture aperture (see Section 3.1.3). This effect is not considered.

- The mechanical model only accounts for localised damage and non-local damage/break of asperities; the impact of asperity damage produced gauge particles are not considered (see Section 3.1.5).

- The proposed correction factors, used to define hydraulic aperture, are purely empirical. The generalisation for a broader class of transports is out of the scope of this report.

3.1.3 Determination of critical aspects

Possibly, the main critical aspect of the chosen methodological approach (Figure 3-1) is the decoupling between mechanical and hydraulic processes. Close to the inlet boundary, water pressure is around 39 kPa, whereas the confining pressure in the unloaded state is around 5.8 kPa (considering an average thickness of the upper slab of 20 cm and a bulk density of 3 000 kg/m³). It turns out that in unloaded conditions, the significantly high water pressure close to the fracture inlet might indeed have caused an initial displacement and rotation of the fracture. This seems to be confirmed by the LVDT sensors (Figure 3-3 and Figure 3-4): some of them (e.g. LVDT 2 and LVDT 3 in the test on the unopened fracture and direction 13) show a negative displacement at the beginning of the experiment.
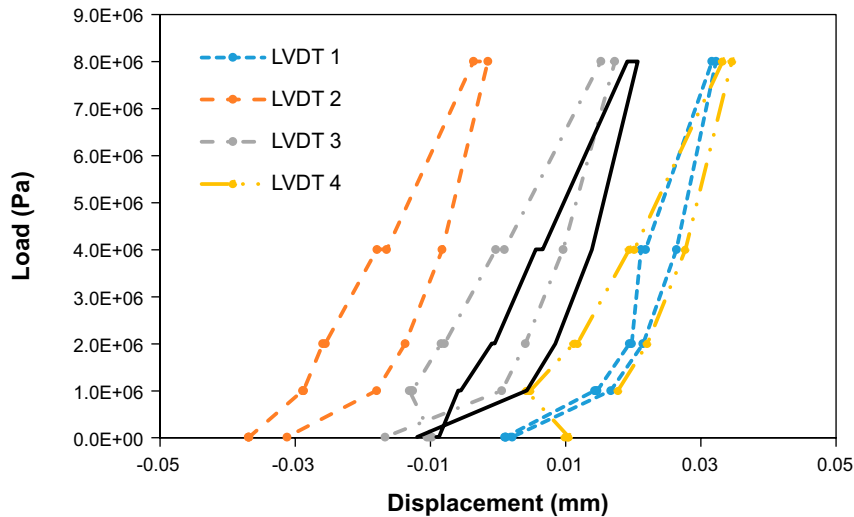
Figure 3-3. *Displacement vs. load for the four different LVDT sensors. The continuous line is the average displacement used for the model calibration. This data was obtained from the HM test on the unopened fracture and direction 13.*
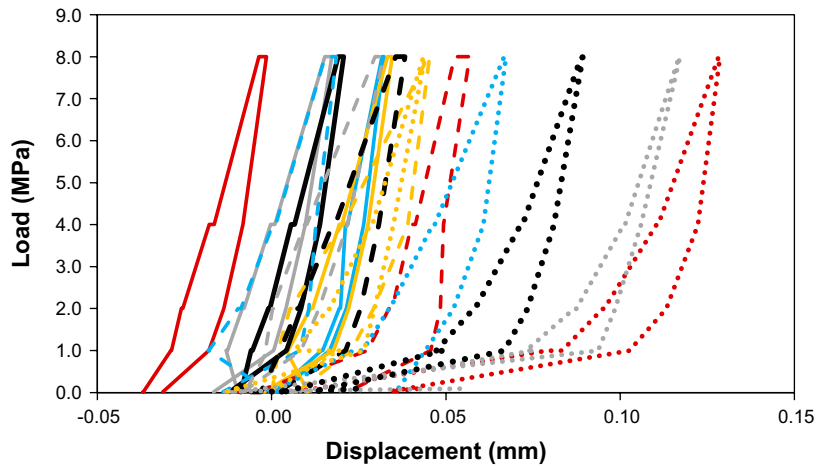
Figure 3-4. *Displacement vs. load for the four different LVDT sensors. Continuous lines are for the HM test on unopened fracture and direction 13; dashed lines are for the HM test on the unopened fracture and direction 24; dotted lines are for the HM test in resealed fracture and direction 24 (only the first cycle is plotted). Blue is LVDT 1, red is LVDT 2, grey is LVDT 3, yellow is LVDT 4 and black is the average LVDT displacement.*

3.1.4 Model parameters

The main mechanical parameters used in the contact model are listed in Table 3-1.

Table 3-1. Parameters used for the contact model. Notice that it has been assumed that $E_1 = E_2 = E$ and $v_1 = v_2 = v$. The Young modulus has been provided in the TD (Bruines, unpublished)[5] whereas the other parameters are plausible values taken from the literature.

Parameter	Value
Young modulus (E)	73.1 GPa
Poisson's ratio (v)	0.32
Hardness (H)	0.1·E (elastic case)
	0.01·E (plastic case)

The initial fracture scan data (*Complete_lower_part_after_first_opening.csv* and *Complete_upper_part_after_first_opening.csv*) have been used to compute the initial fracture aperture. This fracture scan data has been first interpolated to a regular grid of $\Delta x = \Delta y = 5.0 \times 10^{-4}$ m, leading to a total number of 398×399 grid cells using nearest neighbour interpolation. This grid size is coarser than the resolution of the fracture scan data, which is around 0.1–0.2 mm. Sensitivity calculations of the mechanical model have been run with a resolution of 0.125 mm; i.e. the same resolution as the fracture scan data, and the results have shown essentially the same patterns observed with the coarser grid.

The initial fracture aperture includes some contact points, i.e. points where aperture is equal to zero. As the mechanical load is applied, in the mechanical model, other contact points will appear. Contact points are included in the Darcy-based flow simulations (i.e. MODFLOW models) but they essentially do not contribute to flow, since they are assigned a very low permeability value.

The local aperture (δ) has then been computed in this regular grid (which is also used for the contact model) as the difference between the height of the upper surface and the height of the lower surface. A calibration has been required to appropriately fit the measured LVDT displacement. This calibration consisted in reducing all the local aperture values by a constant value (δ_r):

$$\delta_c(\mathbf{x}) = \delta(\mathbf{x}) - \delta_r \qquad\qquad \text{Equation 3-14}$$

What has been considered as successful calibration (Figure 4-1 in Chapter 4) has been obtained by setting $\delta_r = 1.2 \times 10^{-4}$ m. All the grid cells where $\delta_c < 0$ have been considered as contact points and δ_c has been set equal to 0.

The model domain is $L_2 = 0.04$ m², where L is the fracture size. In all the flow calculations a gradient of 20.3 has been considered. This corresponds to a difference in head level between the inlet and outlet boundary of $\Delta h = 4$ m.

The main modelling uncertainties are indeed related to the mapping of the computed fracture aperture to depth averaged local hydraulic parameters (see Section 3.1.2 and Equation 3-12). The cubic law is applied by assuming that water density, ρ, is equal to 1 000 kg/m³ and that water dynamic viscosity, μ, is equal to 8.9×10^{-4} Pa·s.

It is well known that LCL gives biased results when applied to real rough fracture, since it tends to largely overestimate fracture hydraulic properties (e.g. Oron and Berkowitz, 1998). Several correction methods have been proposed (see Table 1 in He et al., 2021); however, most of them are based on correction factors derived from complex topological analyses. Here, the resulting uncertainty is assessed simply by adding a correction factor ($f \leq 1$).

---

[5] Bruines P. SKB Task Force on Modelling of Groundwater Flow and Transport of Solutes: Description of Task 10.2. SKB R-23-10, Svensk Kärnbränslehantering AB, Stockholm, Sweden. Unpublished.

Flowrates are also analysed using the global cubic law:

$$\frac{Q}{\Delta h} = [f \cdot \bar{\delta}]^3 \frac{\rho g}{12 \, \mu} \frac{W}{L}$$

Equation 3-15

where $Q/\Delta h$ is the flowrate per unit drop in head, $\bar{\delta}$ is the effective fracture aperture and W and L are, respectively, the fracture width and length. Notice that $W = L = 0.2$ m.

Reynolds numbers for the different cases have been computed as (Zimmerman et al., 2004):

$$Re = \frac{\rho Q}{\mu W}$$

Equation 3-16

3.1.5 Uncertainty analyses

The main uncertainties of the prediction exercise are related to:

1. The choice of an uncoupled approach, which presumes that hydraulic processes do not affect mechanical closure.

2. The suitability of the laminar flow assumption and cubic law to describe flow at the scale of the considered single fracture.

3. Errors and uncertainties related to high resolution scanning of the two fracture surfaces.

Point 2 above has been addressed in two different ways. The first approach is rather empirical and consists of introducing a correction factor (Equation 3-13 and Equation 3-15) and running a few sensitivity cases (Figure 4-8 and Figure 4-9). The second approach is more rigorous and consists of explicitly resolving fracture aperture and solving the Navier-Stokes equation (see Appendix).

The matrix hardness is an important parameter in the elastic-plastic model, which is not directly measured by experiments on this fracture sample. In the literature, the hardness is often measured by indentation hardness tests for rock samples with smooth surfaces (Kling et al., 2018). However, the hardness behaviour can be influenced by the contact geometry (Li et al., 2009). In a test with smooth surfaces, the hardness is most likely measured under a confined condition. By contrast, the required hardness in the shear model for determining the normal stress-caused plastic deformation at each asperity contact is more likely to be under unconfined conditions. Thus, the adopted hardness value in our shear predictions could be physically reasonable. However, more quantitative analyses, including reliable indentation hardness tests on fracture surfaces with rough asperities, is still required to fully understand the influence of contact geometry on the hardness of rock fractures. Meanwhile, due to the assumption that the rock asperity deforms as an elastic-perfectly plastic material and plastic deformation is confined within a local small area, the non-local damage/break of asperities and the impact of asperity damage produced gauge particles are not considered.

About Point 3 above, this is not addressed in this report but it is briefly discussed in an accompanying paper (Trinchero et al., 2024).

3.2 Prediction and validation of flow along a fracture at different normal loads

3.2.1 Definition of the performance measures and criteria

The primary performance measures have been defined consistently with the TD (Bruines, unpublished)[6]; they are

- Aperture distributions at normal stresses of 0, 1 and 4 MPa.

- Flow rates for 0, 1 and 4 MPa in both the 2-4 and the 1-3 direction.

- Channelling factor, d_{qnet} (Maillot et al., 2016):

$$d_{qnet} = \frac{1}{\sum S_m} \frac{(\sum S_m \cdot v_m)^2}{(\sum S_m \cdot v_m^2)}$$

Equation 3-17

where S_m is the area of each computing grid cell and v_m is the Darcy velocity.

These two performance measures are summarised in Section 3.2.2 whereas additional performance measures and results are provided in Chapter 4.

3.2.2 Task 10.2.2c: Prediction-outcome exercise of flow along an unopened fracture at different normal loads

Histograms and cumulative distribution functions of initial aperture vs. aperture after 1 MPa and 4 MPa have been applied and are shown in Figure 3-5 and Figure 3-6.
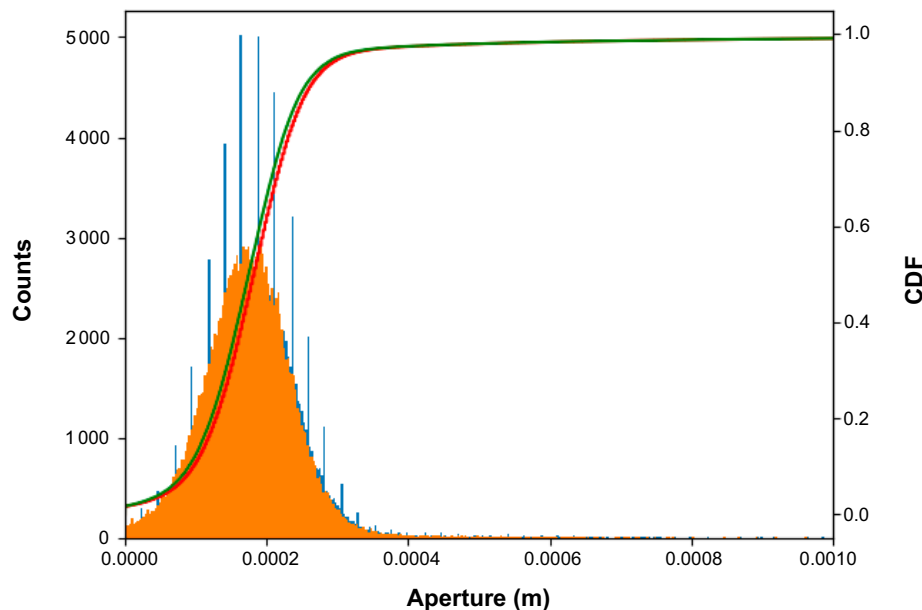
Figure 3-5. *Histograms of aperture distribution for the initial aperture (blue histogram) and for the aperture after 1 MPa has been applied (orange histogram). Cumulative distribution functions are shown in the secondary y-axis for the initial aperture (green curve) and the aperture after 1 MPa has been applied (red curve).*

---

[6] Bruines P. SKB Task Force on Modelling of Groundwater Flow and Transport of Solutes: Description of Task 10.2. SKB R-23-10, Svensk Kärnbränslehantering AB, Stockholm, Sweden. Unpublished.
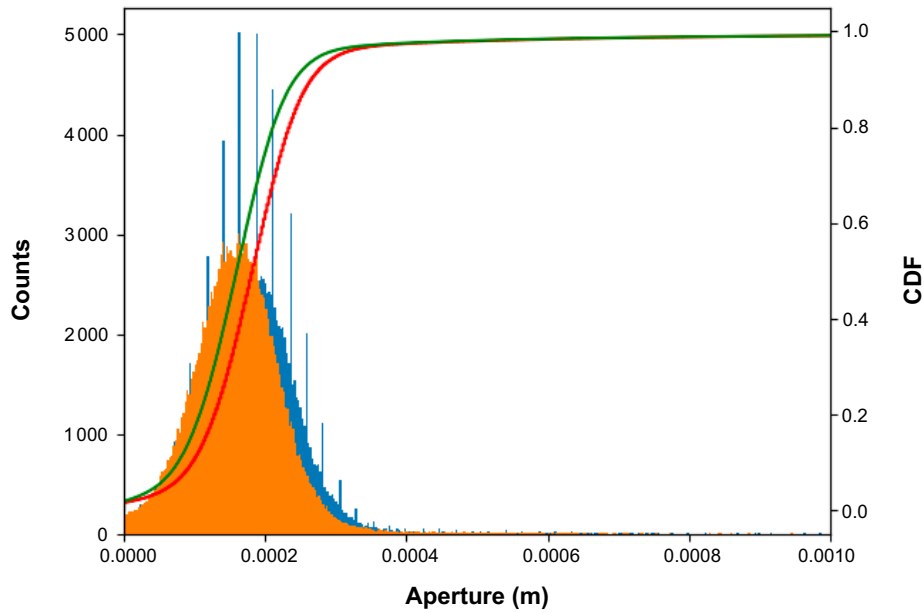
Figure 3-6. *Histograms of aperture distribution for the initial aperture (blue histogram) and for the aperture after 4 MPa has been applied (orange histogram). Cumulative distribution functions are shown in the secondary y-axis for the initial aperture (green curve) and the aperture after 4 MPa has been applied (red curve).*

Table 3-2. First, second and third quantile (Q_1, Q_2 and Q_3), 99th percentile and percentage of contact points for the fracture at the different considered loading states.

Load [MPa]	Q_1 [m]	Q_2 [m]	Q_3 [m]	P_{99} [m]	Contact points [%]
0	1.4×10^{-4}	1.8×10^{-4}	2.2×10^{-4}	9.1×10^{-4}	1.6
1	1.3×10^{-4}	1.7×10^{-4}	2.2×10^{-4}	9.1×10^{-4}	1.7
4	1.2×10^{-4}	1.6×10^{-4}	2.0×10^{-4}	8.9×10^{-4}	1.9

Computed flow rates for 0, 1 and 4 MPa in both the 2-4 and the 1-3 direction are listed in Table 3-3. All these results have been obtained by considering depth-averaged properties based on LCL. Additional calculations have been carried out, where the aperture has been explicitly resolved and the Navier-Stokes equation is solved (see Appendix). So far, in these calculations only the initial aperture, after initial calibration, has been considered. The flow-rate obtained using this approach is $Q_{1-3} = 1.9 \times 10^{-6}$ m³/s. Additional flow rates computed from the sensitivity analyses are shown and discussed in Chapter 4.

Table 3-3. Flow rates and related Reynolds numbers computed at 0, 1 and 4 MPa for 1-3 direction (Q_{1-3}) and 2-4 direction (Q_{2-4}).

Load [MPa]	Q_{3-1} [m³/s]	Q_{2-4} [m³/s]	Re_{3-1} [-]	Re_{2-4} [-]
0	2.0×10^{-5}	1.6×10^{-5}	112	90
1	1.8×10^{-5}	1.4×10^{-5}	101	79
4	1.3×10^{-5}	1.0×10^{-5}	73	56

Channelling factors (Equation 3-17) computed for 0, 1 and 4 MPa in both the 2-4 and the 1-3 direction are listed in Table 3-4.

Table 3-4. Channelling factor (d_{qnet}) for flow direction 3-1 and 2-4.

| Load [MPa]	d_{qnet} 3-1 [-]	d_{qnet} 2-4 [-]
0	0.59	0.61
4	0.57	0.56
8	0.52	0.51

4 Results

4.1 Analysis of the impact of normal load on flow patterns

As explained in Section 3.1.4, the initial aperture (derived from the scan measurement) had to be calibrated. After calibration, a reasonable match is obtained between the computed and the measured average displacement (Figure 4-1).

The resulting initial and final fracture aperture distribution is shown in Figure 4-2. Notice that from now on we refer to the computed fracture aperture at 8 MPa loading level as the final aperture.
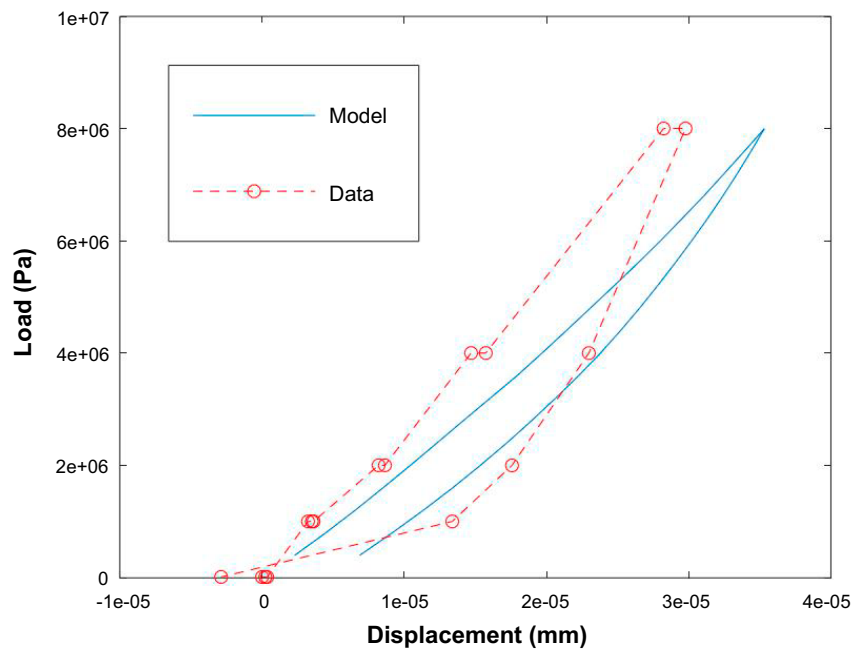

Figure 4-1. *Computed vs. measured average displacement as a function of normal load. The measured displacement is the average of the values of the four LVDT sensors. Data are for the HM test on unopened fracture and direction 1-3.*
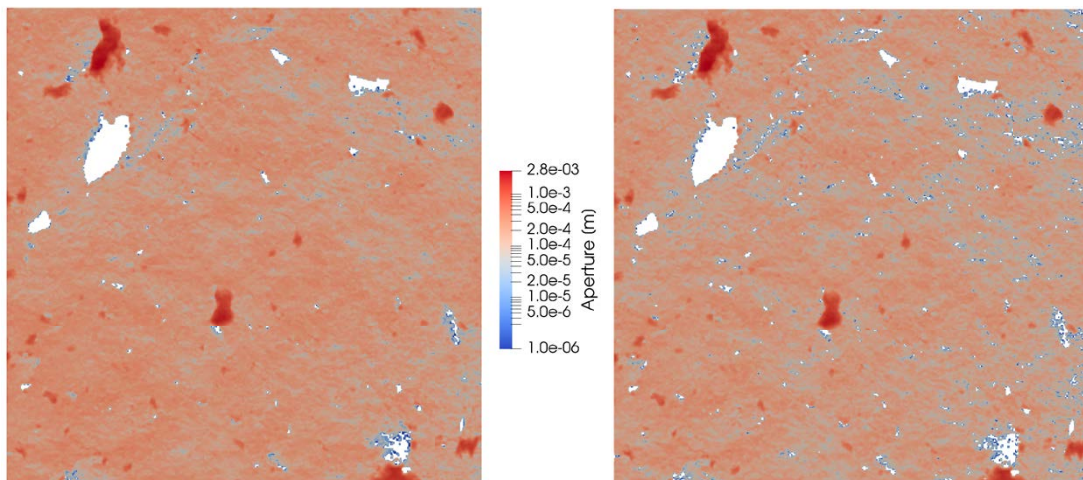

Figure 4-2. *Initial fracture aperture (left) and fracture aperture at 8 MPa loading level (right).*

The changes of flowrate as a function of the normal state computed assuming laminar flow and the LCL for the two assumed flow directions are shown in Figure 4-3. The same results are presented in Figure 4-4 as flowrates per unit change of water head.

Figure 4-5 shows the flowrates computed using the LCL at the different loading states normalised by the corresponding flowrates computed using the Global Cubic Law (GCL) (Equation 3-15) and the median value of fracture aperture. In the same figure the Relative Standard Deviation (RSD) of fracture aperture is also shown.
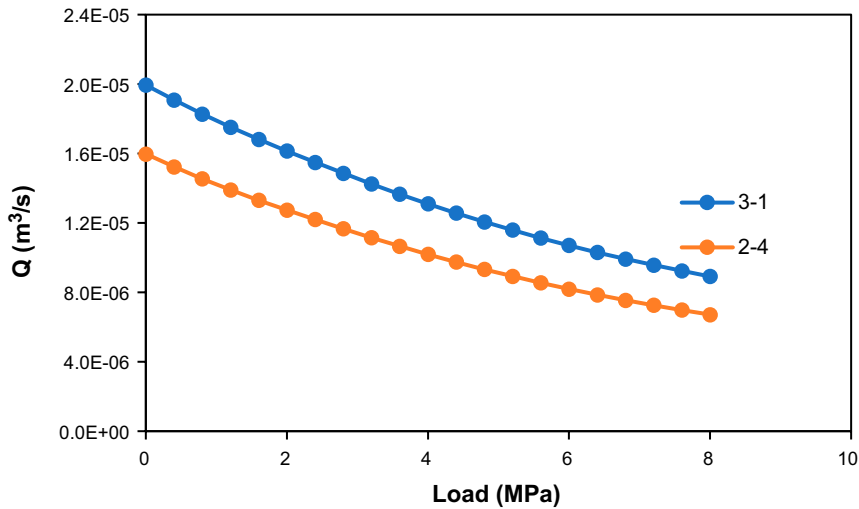
Figure 4-3. *Flowrates computed along the two considered flow directions (1-3 and 2-4) and for the different loading states assuming laminar flow and the LCL.*
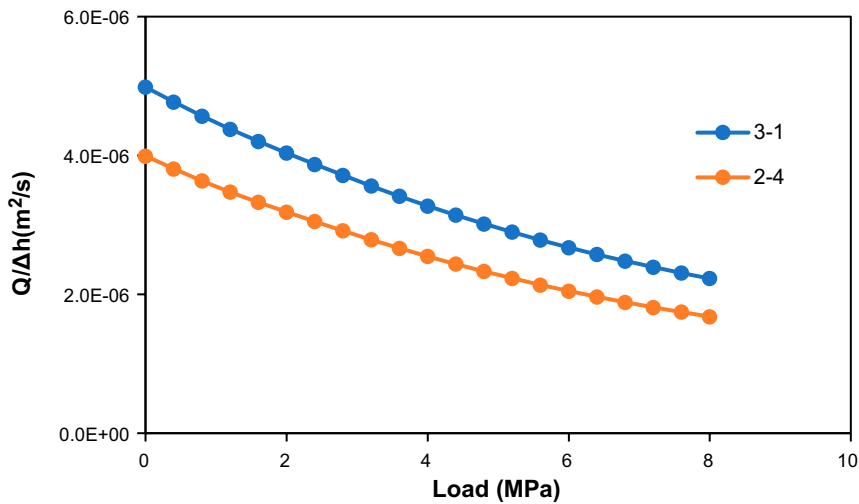

Figure 4-4. *Flowrates per unit drop in head computed along the two considered flow directions (1-3 and 2-4) and for the different loading states assuming laminar flow and the LCL.*
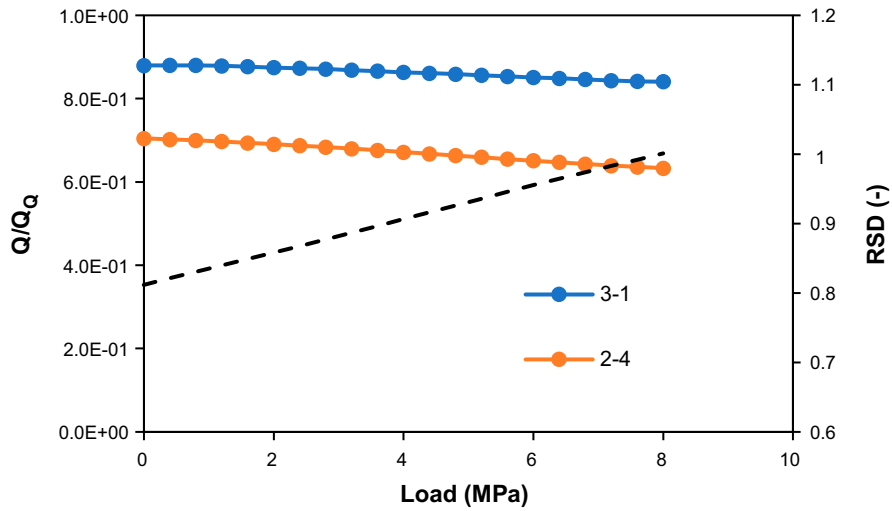
Figure 4-5. *Flowrates (Q) computed along the two considered flow directions (1-3 and 2-4) and for the different loading states assuming laminar flow and the LCL. Flowrates are normalised by the corresponding flowrate obtained using GCL and the median of fracture aperture at the corresponding loading state (Q_0). The dashed line shows the Relative Standard Deviation (RSD) of the fracture aperture.*

Groundwater velocity distributions (magnitude of the velocity vector, $\|\mathbf{v}\|$) have been visually analysed for the 1-3 and 2-4 flow direction and the different loading states. Velocities were normalised by the corresponding velocity based on the GCL model and the median fracture aperture (v_c). Results for the 3-1 direction are shown in Figure 4-6.
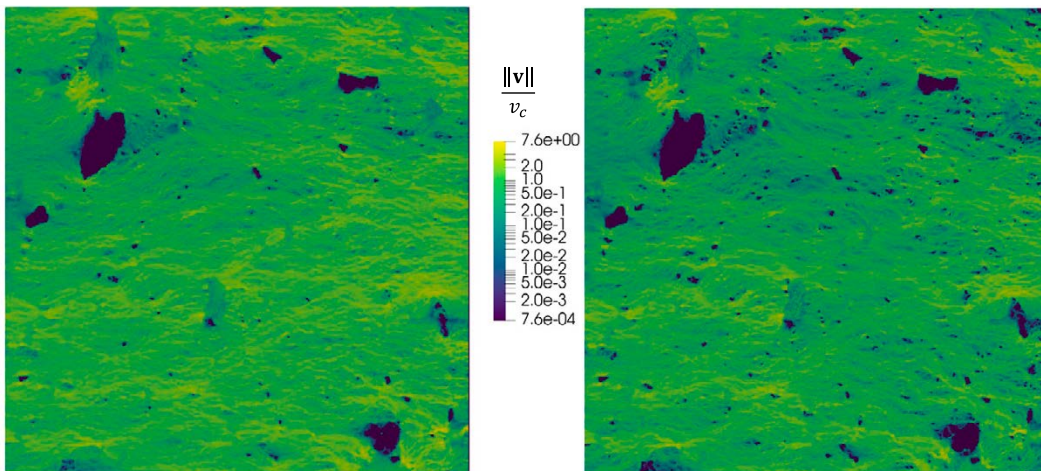

Figure 4-6. *Flow in 1-3 direction. Normalised magnitude of velocity for (left) the initial aperture and (right) the final aperture (8 MPa loading level).*

Figure 4-7 shows the evolution of the channelling indicator, d_{qnet} (Equation 3-17) as a function of the normal state and for the two principal directions. Notice that a decrease in d_{qnet} implies a general increase of channelling, which basically means that channelling increases with normal load.

Sensitivity of Q to fracture aperture has been analysed using the modified LCL and Equation 3-13 and considering different correction factors (spanning from 1.0 to 0.1) and different loading levels. Results are summarised in Figure 4-8. Flowrates span from a maximum of 2.0×10^{-5} m³/s (initial fracture aperture and $f = 1$) to a minimum of 9×10^{-9} m³/s.

Sensitivity of Q to fracture aperture has been analysed using GCL, Equation 3-15. A minimum and maximum value of $\bar{\delta}$ have been chosen based on the different quantiles listed in Table 3-2. More specifically, the minimum $\bar{\delta}$ is set equal to Q_1 at 4 MPa whereas the maximum fracture aperture is set equal to Q_3 at 0 MPa. Three different values of correction factor have been considered. The minimum computed flowrate is 6.3×10^{-9} m³/s whereas the maximum is 3.9×10^{-5} m³/s.
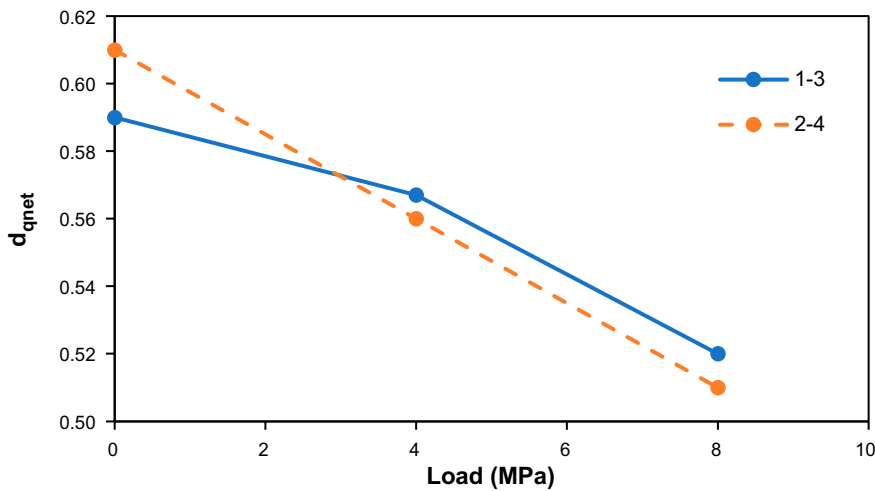
Figure 4-7. *Channelling indicator (d_{qnet}) as a function of the loading state for the two considered flow directions.*
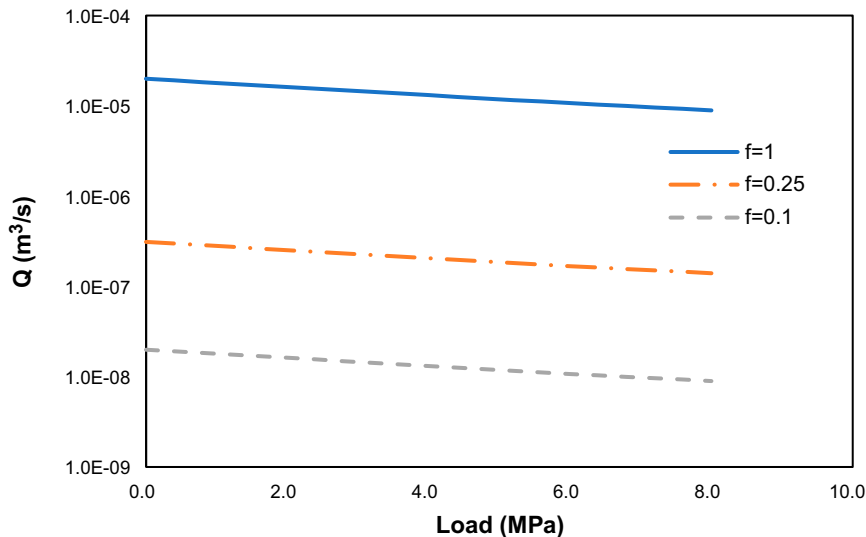
Figure 4-8. *Sensitivity analysis using LCL (flow direction 1-3): changes in computed flowrates as a function of the correction factor (f).*
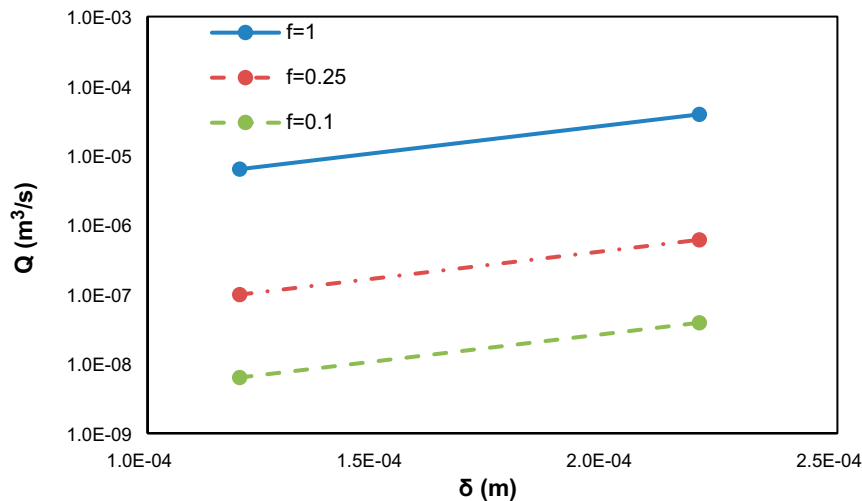
Figure 4-9. *Sensitivity analysis using GCL: changes in computed flowrates as a function of the effective fracture aperture (δ̄) and correction factor (f).*

## 4.2 Comparison of blind predictions with experimental data

Experimental flow results were delivered to the modelling groups on January 20th, 2023, i.e. after all the calculations presented in this report were completed and preliminarily reported. In this short section, the computed flowrates are visually compared with the experimental data. For the sake of completeness, the following numerical results are included in each plot (see Figure 4-10 to Figure 4-11):

- Groundwater flow simulations performed using the LCL assumption and the different fracture apertures representative of the different normal loads (Equation 3-12; continuous blue lines in the plots).

- Groundwater flow simulations performed using the LCL assumption with the correction factor *f* and the different fracture apertures representative of the different normal loads (Equation 3-13; dashed and dashed dotted lines in the plots).

- Navier-Stokes equation solved by explicitly resolving for the initial fracture aperture (Appendix; dots in the plots).

The results of the simulations show that when LCL is applied directly to the different fracture aperture fields, the flow rates are overestimated by more than three orders of magnitude. It is noticed that the initial calibrated aperture, when used in conjunction with a CFD model, provides flow rate estimates that are in agreement with the experimental values. Therefore, the overestimation is indeed related to the assumption underlying the LCL simplification. A correction factor *f* of 0.1 (i.e. a hydraulic aperture equal to one tenth of the mechanical aperture) provides a much better representation of the flowrates at the initial state but it does not reproduce well the observed decrease in flowrate as the normal load increases. The reason for this is to be found in the mechanical model, which shows some mismatch in the representation of normal displacements (Figure 4-1). In Trinchero et al. (2024) a more accurate mechanical simulation is presented and based on that it is shown that the LCL with a correction factor *f* = 0.2 can reproduce well the trend observed in the experimental data during the entire loading cycle.
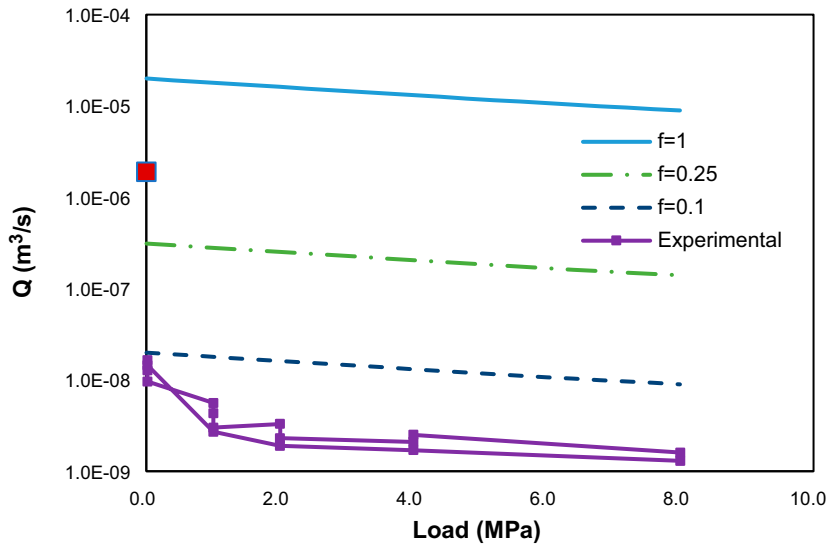
Figure 4-10. *Flowrates along 1-3 direction computed using LCL and different correction factors. The purple continuous dotted line shows the experimental results along direction 1-3 for the unopened fracture. The red dot is the flowrate computed using CFD simulations.*
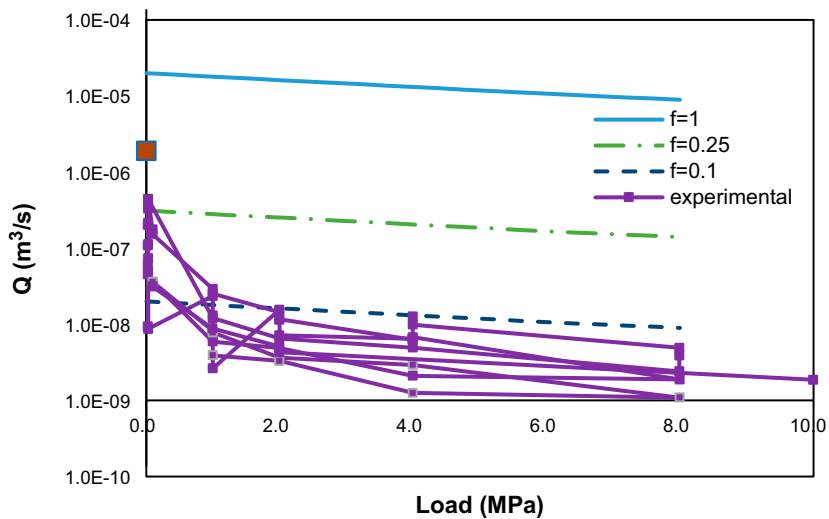
Figure 4-11. *Flowrates along 1-3 direction computed using LCL and different correction factors. The purple continuous dotted lines are the experimenta flowrate along direction 1-3 for the different cycles performed on the resealed fracture. The red dot is the flowrate computed using CFD simulations.*

5 Discussion, summary and conclusions

5.1 Discussion

The main calculations summarised in this report are based on the assumption of the validity of the local cubic law (LCL); that is, it is assumed that local aperture can be converted to local transmissivity, thus producing a 2D depth-averaged representation of fracture internal variability. The cubic law is based on the hypothesis of laminar flow. The latter seems to be an appropriate assumption given the very low flowrates obtained in the experimental study. However, evidence exists that even at low Reynolds numbers the cubic law is unsuited to describe flow in natural rough fractures, since it tends to largely overestimate fracture hydraulic properties (e.g. Oron and Berkowitz, 1998). The results presented here seem to confirm this previous finding, since computed flowrates exceed experimental observations by about three orders of magnitude. However, it should be noted that part of this overestimation might be caused by uncertainties related to the initial fracture aperture.

A correction factor is proposed here, which consists in scaling the local fracture aperture by a scaling factor. This is essentially consistent with the distinction made in SR-site between hydraulic and transport aperture (see Selroos et al., 2022 and references therein), with the latter being set equal to one tenth of the former. In the results presented here, the LCL models based on the calibrated scaling factor ($f = 0.1$) do not reproduce very well the decreasing trend in flowrate associated with the increase in normal load. However, this is attributed to the poor calibration of the mechanical model. In the companion paper (Trinchero et al., 2024), where a more careful mechanical calibration was performed, the modified LCL models, based on a different correction factor ($f = 0.2$), capture the aforementioned trend, indicating that the approach is valid for extrapolating results to conditions different from those used to derive the empirical scaling factor.

Predictions performed with a 3D Navier-Stokes based model provides lower flowrates compared with the base case LCL simulation, but they still do overpredict experimental results, by about two orders of magnitude. Therefore, this initial aperture has been here calibrated against the average LVDT displacement. Nonetheless, this calibration does not account for possible differential displacements observed in the early stage of the experiment, when water pressure close to the inlet exceeds residual confinement pressure (Figure 3-3). This possible mechanical rotation, which is not accounted for in our models, adds additional uncertainty to the presented results.

5.2 Conclusions

An important conclusion of this work and the accompanying paper (Trinchero et al., 2024) is that geometrical information on fracture aperture distribution is likely to be highly biased, no matter how accurate the sample handling and associated measurements are. Therefore, for a successful pragmatic validation modelling, additional data including such as flowrates, tracer test breakthrough curves (if any) and possibly electrical resistivity measurements, should be included to constrain the initial conditions and thus derive a reliable starting point for the model. Indeed, the difficulty in deriving initial conditions is indeed related to the non-linear dependence between fracture aperture and flowrates (i.e. small uncertainties in fracture aperture lead to large uncertainties in flowrates). The practical impossibility to thoroughly characterise the void space of the fracture is related to its spatial scales (from mm down to micro meter scale for the narrower regions of fracture aperture). About this point, it is worthwhile that fracture scan data provided to the modellers were obtained by opening the fracture, which led to material loss thus adding additional uncertainty. Furthermore, the realignment of the two fracture surfaces is and error prone exercise.

Despite the underlying uncertainties, the results presented here clearly show that direct mapping local (geometrical) fracture aperture to local transmissivity values is an inadequate approach that significantly overestimates flowrates. This is not surprising, since there is an extensive body of literature where this has been pointed out (see He et al., 2021 and references therein).

Further improvement of the model entails:

1. Extending the Navier-Stokes models to the inverse modelling of the HM experiment, so that internal void space is properly captured; and

2. Carry out a systematic analysis of the corrected LCL in order to establish a pragmatic approach for use in large-scale flow and transport simulations.

About point 2 above, this systematic analysis could be done by analysing correction factors for a broad range of "granitic fractures", trying then to correlate them to specific metrics of fracture roughness, such as the roughness exponent of the JRC. This would however require a tradeoff between the large data-set of fractures required to characterize realistic ranges of JRC and the computational costs of the required simulations.

Recommendations

Do you have any recommendation to other modelling groups and future studies?

Regular communication among modelling groups is important to ensure that all relevant information and experience is shared. This can help to avoid duplication of effort and ensure that best practices are shared across different groups.

In addition, benchmark exercises can be useful to ensure that modelling tools are set up correctly and that no errors are carried forward into the main modelling activity. This can help to ensure that the final results are accurate and reliable and can help to build confidence in the modelling approach.

Overall, effective communication and quality control are essential for successful modelling efforts. By following these basic principles, modelling groups can improve the accuracy and reliability of their work.

What could have been done differently to obtain better overall results?

It is difficult to say. One option that could have been considered is to use a fluid with lower viscosity, so that lower hydraulic gradients could have been used. This would have decreased the uncertainty related to possible rotation of the fracture induced by the high pressure at the fracture inlet. It would also have been interesting to complement the results with electrical resistivity measurements, although I think that this has been discarded because of the underlying complexities.

References

SKB's (Svensk Kärnbränslehantering AB) publications can be found at www.skb.com/publications.

Barton N, Choubey V, 1977. The shear strength of rock joints in theory and practice. Rock mechanics, 10, pp.1–54.

Fernandez-Garcia D, Illangasekare, T H, Rajaram H, 2005. Differences in the scale dependence of dispersivity and retardation factors estimated from forced-gradient and uniform flow tracer tests in three-dimensional physically and chemically heterogeneous porous mediaart. no. W03012. Water Resources Research 41, 3012–3012.

Godio M, Jacobsson L, 2024. Experimental study on the hydromechanical behaviour of a natural unperturbed fracture under normal loading: Derivation of the equivalent hydraulic aperture and its digital reconstruction. RISE Report 2024:8. ISBN 978-91-89896-49-9. http://urn.kb.se/resolve?urn=urn:nbn:se:diva-71540

Harbaugh A, Banta E, Hill M, McDonald M, 2000. MODFLOW-2000 The US Geological Survey modular ground-water model-User guide to modularization concepts and the ground-water flow process. US Geological Survey Open-File Report 00-92 121.

He X, Sinan M, Kwak H, Hoteit H, 2021. A corrected cubic law for single-phase laminar flow through rough-walled fractures. Advances in Water Resources 154, 103984. https://doi.org/10.1016/j.advwatres.2021.103984

Jacobsson L, Godio M, 2023. Measuring the hydraulic transmissivity of a rock joint under varying normal load, Rock and Fracture Mechanics in Rock Engineering and Mining (EUROCK), September 12–15, 2022, Espoo, Finland, IOP Conf. Ser.: Earth Environ. Sci. 1124 012050. https://doi.org/10.1088/1755-1315/1124/1/012050

Kling T, Vogler D, Pastewka L, Amann F, Blum P, 2018. Numerical Simulations and Validation of Contact Mechanics in a Granodiorite Fracture. Rock Mechanics and Rock Engineering 51, 2805–2824. https://doi.org/10.1007/s00603-018-1498-x

Li M, Chen W, Cheng Y-T, Cheng, C-M, 2009. Influence of contact geometry on hardness behavior in nano-indentation. Vacuum 84, 315–320. https://doi.org/10.1016/j.vacuum.2009.07.001

Li B, Cui X, Zou L, Cvetkovic V, 2021. On the Relationship Between Normal Stiffness and Permeability of Rock Fractures. Geophysical Research Letters 48, e2021GL095593. https://doi.org/10.1029/2021GL095593

Maillot J, Davy P, Goc R L, Darcel C, de Dreuzy J R, 2016. Connectivity, permeability, and channeling in randomly distributed and kinematically defined discrete fracture network models. Water Resources Research 52, 8526–8545. https://doi.org/10.1002/2016WR018973

Oron A P, Berkowitz B, 1998. Flow in rock fractures: The local cubic law assumption reexamined. Water Resources Research 34, 2811–2825. https://doi.org/10.1029/98WR02285

Polonsky I A, Keer L M, 1999. A numerical method for solving rough contact problems based on the multi-level multi-summation and conjugate gradient techniques. Wear 231, 206–219. https://doi.org/10.1016/S0043-1648(99)00113-1

Selroos J O, Mas Ivars D, Munier R, Hartley L, Libby S, Davy P, Darcel C, Trinchero P, 2022. Methodology for discrete fracture network modelling of the Forsmark site. Part 1 – concepts, data and interpretation methods. SKB R-20-11, Svensk Kärnbränslehantering AB, Stockholm, Sweden.

Tian X, Bhushan B, 1996. A Numerical Three-Dimensional Model for the Contact of Rough Surfaces by Variational Principle. Journal of Tribology 118, 33–42. https://doi.org/10.1115/1.2837089

Trinchero P, Zou L, de La Iglesia, M, Iraola A, Bruines P, Deissmann G, 2024. Experimental and numerical analysis of flow through a natural rough fracture subject to normal loading. Scientific reports, 14(1), 5587.

Warming R F, Beam R M, 1976. Upwind Second-Order Difference Schemes and Applications in Aerodynamic Flows. AIAA Journal 14, 1241–1249. https://doi.org/10.2514/3.61457

Witherspoon P A, Wang J S Y, Iwai K, Gale J E, 1980. Validity of Cubic Law for fluid flow in a deformable rock fracture. Water Resources Research 16, 1016–1024. https://doi.org/10.1029/WR016i006p01016

Zimmerman R W, Al-Yaarubi A, Pain C C, Grattoni CA, 2004. Non-linear regimes of fluid flow in rock fractures. International Journal of Rock Mechanics and Mining Sciences 41, 163–169. https://doi.org/10.1016/j.ijrmms.2004.03.036

Zou L, Li B, Mo Y, Cvetkovic V, 2020. A High-Resolution Contact Analysis of Rough-Walled Crystalline Rock Fractures Subject to Normal Stress. Rock Mechanics and Rock Engineering 53, 2141–2155. https://doi.org/10.1007/s00603-019-02034-w

Modelling approach based on the Navier-Stokes equations

An alternative modelling approach to the one shown in Chapter 3, consists in explicitly resolving fracture aperture and solving the Navier-Stokes equation. All this modelling work was conducted using the finite-volume numerical code OpenFOAM.

The initial fracture aperture was discretised using an orthohedral mesh consisting of more than 50 million elements using the mesh generation tool called snappyHexMesh (Figure A-1). The mesh has higher refinement in the borders close to contact points. An upwind second-order difference scheme is used for both velocity and pressure (Warming and Beam, 1976). The PIMPLE (Pressure-Implicit with Splitting of Operators, Semi-Implicit Method for Pressure-Linked Equations) solver is used for the calculations. PIMPLE uses a semi-implicit approach to handle the pressure-velocity coupling and employs a pressure-correction approach to ensure that the pressure and velocity fields are consistent with each other. In each time step, the solver alternates between solving for a velocity predictor field and correcting the pressure field. These steps are repeated until the solution converges to a certain criterion. The linear solver employed was the geometric-algebraic multi-grid (GAMG) solver.
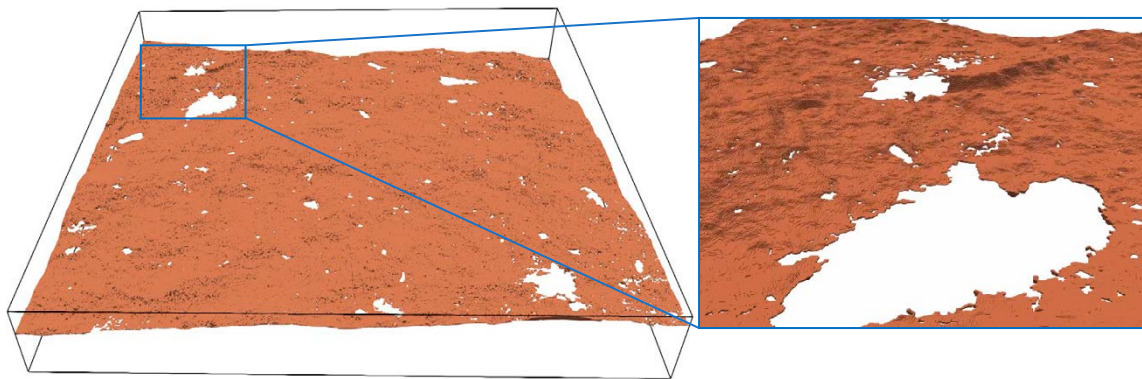
Figure A-1. *Details of the initial fracture aperture as implemented in OpenFOAM.*

The Navier-Stokes equation consists in solving simultaneously for the mass and momentum balance equations, respectively:

$$\nabla \cdot \boldsymbol{v} = 0 \qquad\qquad \text{Equation A-1}$$

and

$$\frac{\partial \rho \boldsymbol{v}}{\partial t} + \nabla \cdot (\rho \boldsymbol{v}\boldsymbol{v}) = -\nabla p + \rho \boldsymbol{g} + \nabla \mu (\nabla \boldsymbol{v} + \nabla^{t} \boldsymbol{v}) \qquad\qquad \text{Equation A-2}$$

where $\boldsymbol{v}$ is the velocity vector and the other variables are as in Section 3.1.4. Notice that Equation A-1 presumes that the fluid is incompressible.

It is assumed that fluid particles at the solid wall cannot move tangentially, and thus a no-slip condition is applied on all boundaries:

$$\boldsymbol{v} = 0 \qquad\qquad \text{Equation A-3}$$

except for boundary 3 and boundary 1 (Figure 3-2) where a constant pressure is applied, with a difference of pressure equal to 39 240 Pa. A parabolic profile of velocity is assumed at the boundaries.

SKB is responsible for managing spent nuclear fuel and radioactive waste produced by the Swedish nuclear power plants such that man and the environment are protected in the near and distant future.

skb.se